

SUBSTELLAR OBJECTS IN NEARBY YOUNG CLUSTERS (SONYC) IX: THE PLANETARY-MASS DOMAIN OF CHAMAELEON-I AND UPDATED MASS FUNCTION IN LUPUS-3 *

KORALJKA MUŽIĆ^{1,**}, ALEXANDER SCHOLZ², VINCENT C. GEERS^{3,4}, RAY JAYAWARDHANA⁵

Draft version November 9, 2021

ABSTRACT

Substellar Objects in Nearby Young Clusters – SONYC – is a survey program to investigate the frequency and properties of substellar objects in nearby star-forming regions. We present new spectroscopic follow-up of candidate members in Chamaeleon-I (~ 2 Myr, 160 pc) and Lupus 3 (~ 1 Myr, 200 pc), identified in our earlier works. We obtained 34 new spectra ($1.5 - 2.4 \mu\text{m}$, $R \sim 600$), and identified two probable members in each of the two regions. These include a new probable brown dwarf in Lupus 3 (NIR spectral type M7.5 and $T_{\text{eff}} = 2800$ K), and an L3 ($T_{\text{eff}} = 2200$ K) brown dwarf in Cha-I, with the mass below the deuterium-burning limit. Spectroscopic follow-up of our photometric and proper motion candidates in Lupus 3 is almost complete ($> 90\%$), and we conclude that there are very few new substellar objects left to be found in this region, down to $0.01 - 0.02 M_{\odot}$ and $A_V \leq 5$. The low-mass portion of the mass function in the two clusters can be expressed in the power-law form $dN/dM \propto M^{-\alpha}$, with $\alpha \sim 0.7$, in agreement with surveys in other regions. In Lupus 3 we observe a possible flattening of the power-law IMF in the substellar regime: this region seems to produce fewer brown dwarfs relative to other clusters. The IMF in Cha-I shows a monotonic behavior across the deuterium-burning limit, consistent with the same power law extending down to $4 - 9$ Jupiter masses. We estimate that objects below the deuterium-burning limit contribute of the order $5 - 15\%$ to the total number of Cha-I members.

Subject headings: stars: formation, low-mass, brown dwarfs, mass function

1. INTRODUCTION

SONYC - short for *Substellar Objects in Nearby Young Clusters* - is a comprehensive project aiming to provide a complete, unbiased census of substellar population down to a few Jupiter masses in young star forming regions. The survey is based on extremely deep optical- and near-infrared wide-field imaging, combined with the Two Micron All Sky Survey (2MASS) and *Spitzer* photometry catalogs, which are correlated to create catalogs of substellar candidates and used to identify targets for extensive spectroscopic follow-up. To further facilitate candidate selection, in Mužić et al. (2014) we also performed a proper motion analysis of the Lupus 3 star forming region. While the candidate selection based on optical and near-infrared photometry helps to avoid biases introduced by the mid-infrared selection (only objects with disks), or methane-imaging (only T-dwarfs), it comes with a cost of relatively large candidate lists affected by significant background contamination. Spectroscopic follow-up is therefore a necessary prerequisite to reliably

characterize the low mass population in young star forming regions.

Thanks to our SONYC survey and the efforts of other groups, the substellar Initial Mass Function (IMF) is now well characterized down to $\sim 0.01 M_{\odot}$. The ratio of the number of stars with respect to brown dwarfs lies between 2 and 6 (Scholz et al. 2013), and the power-law slope of the mass function is $\alpha \sim 0.6$ ($dN/dM \propto M^{-\alpha}$; see Scholz et al. 2012a; Offner et al. 2014 for a summary). It is clear by now that the mass function in young clusters extends below the deuterium-burning (D-burning) limit at $\sim 13 M_{\text{Jup}}$, as a handful of early L-type dwarfs have been spectroscopically confirmed in NGC1333 (Scholz et al. 2012a), ρ Oph (Alves de Oliveira et al. 2012), λ Ori (Bayo et al. 2011), σ Ori (Zapatero Osorio et al. 2000, 2013), Orion (Ingraham et al. 2014), and Cha-I (Luhman et al. 2008). However, the majority of the current surveys are complete down to $\sim 10 M_{\text{Jup}}$, leaving the mass function in the planetary-mass regime still poorly constrained. The surveys that extend to lower masses are mostly based on photometry, and still await spectroscopic follow-up. The SONYC study in NGC 1333 (Scholz et al. 2012b) is unique in this sense, as we obtained spectra of more than 85% of all photometric very-low-mass (VLM) candidates down to $\lesssim 0.005 M_{\odot}$. We find that the free-floating objects with planetary masses are rare, 20-50 times less numerous than stars (for planetary mass objects in range $0.006 - 0.015 M_{\odot}$, and stars below $1 M_{\odot}$). The mass spectrum in NGC 1333 below $0.6 M_{\odot}$ is well described by a power-law form $dN/dM \propto M^{-\alpha}$, with $\alpha \approx 0.6$, and possibly requires lower values of α in the planetary-mass domain. In σ Ori, Peña Ramírez et al. (2012) find the same slope for the mass interval $0.25 - 0.004 M_{\odot}$, and also suggest a

kmuzic@eso.org

¹ European Southern Observatory, Alonso de Córdova 3107, Casilla 19, Santiago, 19001, Chile² School of Physics & Astronomy, St. Andrews University, North Haugh, St Andrews KY16 9SS, United Kingdom³ UK Astronomy Technology Centre, Royal Observatory Edinburgh, Blackford Hill, Edinburgh, EH9 3HJ, United Kingdom⁴ School of Cosmic Physics, Dublin Institute for Advanced Studies, 31 Fitzwilliam Place, Dublin 2, Ireland⁵ Faculty of Science, York University, 355 Lumbers Building, 4700 Keele Street, Toronto, ON M3J 1P2, Canada

* Based on observations collected at the European Southern Observatory under the program 093.C-0050(A).

** Present address: Nucleo de Astronomía, Facultad de Ingeniería, Universidad Diego Portales, Av. Ejercito 441, Santiago, Chile

possibly lower α below $0.004M_{\odot}$. While this result still awaits spectroscopic confirmation, three T-dwarf candidates towards σ Ori have been classified as likely non-members (Peña Ramírez et al. 2015), suggesting that the mass function in this cluster might have a cut-off at $\sim 4 M_{Jup}$. In the central part of Upper Scorpius, spectroscopy of L-type candidates (Lodieu et al. 2011) and proper motions of T-type candidates (Lodieu et al. 2013b) favor a turn-down of the mass function below $10 - 4 M_{Jup}$, depending on the age assigned to the cluster, and the models used. In another photometric survey probing the planetary-mass range in the same region, but over much larger field, Lodieu (2013) concludes that the mass function (in the log-normal form) is likely decreasing in the planetary-mass regime, although the flat function cannot be discarded at this point. A proper-motion and/or spectroscopic analysis of the candidate members is needed before drawing a firmer conclusion.

The surveys in star forming regions thus far are possibly in conflict with the claims of the microlensing study by Sumi et al. (2011), who suggest that the unbound or wide-orbit Jupiter-mass objects are almost twice as common as main sequence stars. One possible mechanism for the formation of objects of this kind might be ejection of BDs, and/or star forming clumps through close encounters in the early stages of cluster formation. However, the typical ejection velocities produced by simulations (e.g. Bate 2009, 2012; Basu & Vorobyov 2012; Reipurth et al. 2010) of up to a few km s^{-1} might result in a population of BDs distributed at the outskirts of the clusters, but not very far from it. Certainly some objects at the tail of the velocity distribution might escape even further, but this cannot be a substantial number. For example, at the end of the cluster simulation in Bate (2009), only about 17% of the low-mass stars and BDs are at the distances beyond the 80%-mass radius of the cluster. Therefore, if the microlensing result holds, the objects they probe should have masses below $\sim 0.005 M_{\odot}$, and their over-abundances would favor a different formation scenario from the one forming the non-D-burning brown dwarfs in young clusters.

Within SONYC, we have investigated the IMF in the two young star forming regions, Chamaeleon-I (hereafter Cha-I; Mužić et al. 2011), and Lupus 3 (Mužić et al. 2014). In this paper we present the second spectroscopic follow-up of the SONYC candidates in these two regions. Based on this more complete set of follow-up spectra, we can better constrain the properties of the IMF at the low-mass end. In Cha-I specifically, we target the candidates expected to have masses below the D-burning limit, in order to derive more definitive conclusions that contribute to the ongoing discussion about the IMF in this mass regime.

In Section 2 we give a summary of our previous work in the two regions, describing in detail the candidate lists and the first spectroscopic follow-up. In Section 2.3 we present the new spectroscopic follow-up with SofI/NTT. The analysis of the spectra is presented in Section 3. The results are discussed in Section 4. Finally, we summarize the main conclusions in Section 5.

2. CANDIDATE LISTS AND SPECTROSCOPIC FOLLOW-UP

In this section we outline previous SONYC campaigns in Cha-I (Mužić et al. 2011), and Lupus 3 (Mužić et al.

TABLE 1
OVERVIEW OF THE VARIOUS SAMPLES IN CHA-I AND LUPUS 3
USED IN THIS PAPER

Sample	No. ^a
Chamaeleon-I	
Candidates selected from Iz diagram	142/106
with spectra from VIMOS	18/18
with spectra from SofI	15/15
confirmed VLM objects by VIMOS spectra	7/7
confirmed VLM objects by SofI spectra	2/2
confirmed VLM objects by other groups ^b	9/9
rejected as VLM objects by our spectra	24/24
rejected as VLM objects by other groups ^b	4/4
Lupus 3	
Candidates selected from iJ diagram ^c	372/337
with spectra from VIMOS	123/112
with spectra from SofI	19/19
confirmed young VLM objects by VIMOS spectra	7/7
confirmed young VLM objects by SofI spectra	2/2
confirmed young VLM objects by other groups ^b	1/1
Candidates from “IJ-pm” sample ^d	58/53
with spectra from VIMOS	32/31
with spectra from SofI	19/19
confirmed young VLM objects by VIMOS spectra	7/7
confirmed young VLM objects by SofI spectra	2/2
confirmed young VLM objects by other groups	0/0

^a total number/above the completeness limit

^b in addition to the members confirmed/rejected by our spectra

^c all photometric candidates, including the “IJ-pm” sample

^d iJ and proper motion candidates

2014), as the analysis presented in this work is a continuation of our past efforts. We give a summary of the candidate lists for the two regions, as well as a detailed description of the second follow-up with SofI/NTT. In Table 1 we provide an overview of the candidate samples used for the analysis presented in Section 4. For each entry, we give the total number of objects, and the number of objects that are brighter than the completeness limit in each of the two surveys. The latter is important since we can derive firm statistical conclusions on the shape of the IMF only in the region where our surveys can be considered complete.

2.1. Chamaeleon-I

While the Cha-I star forming region spreads over several square degrees on the sky, more than 80% of the known members lie within a $\sim 1 \text{ deg}^2$ central stripe (see Luhman 2007). The SONYC photometric survey provided deep images of a part of this area, covering in total $\sim 0.25 \text{ deg}^2$. Our fields contain 38% of the Cha-I population according to the most complete census to date presented in Luhman (2007). Our photometric analysis was based on optical and near-infrared catalogs in I , z , J , and Ks bands⁸. A list of candidate members of Cha-I was selected from the $(I - z, I)$ color-magnitude diagram (CMD), representing a natural extension of the previously known members towards fainter magnitudes.

⁸ Throughout this paper, I stands for Cousins I , and i for DENIS i -band passband. NIR photometry is in the 2MASS system. The z -band photometry was not absolutely calibrated, and is only used to separate the red from the blue sources in the $(I - z)$ color space (see Mužić et al. 2011 for details).

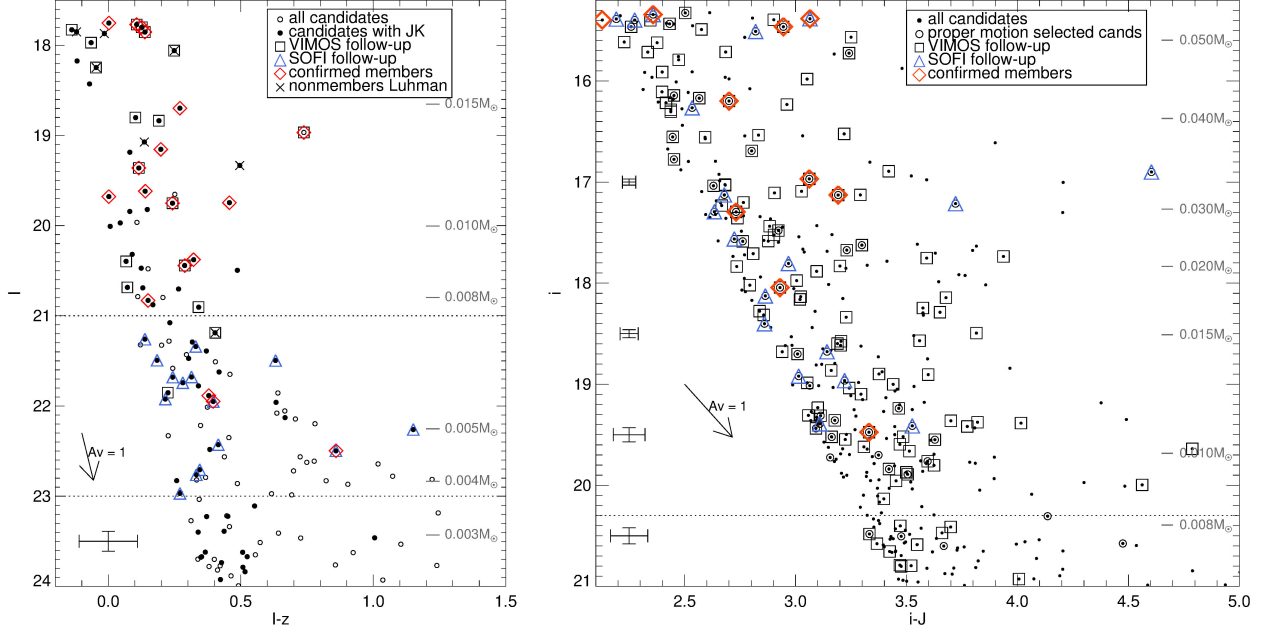


FIG. 1.— **Left:** Color-magnitude diagram showing candidate members of Cha-I (open circles). The filled circles represent those also found in our NIR catalog. The sources observed in two spectroscopic campaigns are shown as black squares (VIMOS/VLT), and blue triangles (Sofi/NTT). The confirmed members of Cha-I are marked with red diamonds, and those classified as non-members in Luhman (2004) with crosses. The horizontal lines in the left panel mark the upper limit for the Sofi follow-up (at $I = 21$), and the I -band completeness limit ($I = 23$). **Right:** Color-magnitude diagram showing candidate members in Lupus 3 (dots). Proper motion candidates are additionally marked with open circles. The remaining symbols are the same as in the left panel. 1σ photometric uncertainties are shown on the left-hand side of the plot. The expected object masses at $A_V = 0$ according to the BT-Settl models are shown on the right-hand side of each plot, for an age of 2 Myrs in Cha-I, and 1 Myr in Lupus 3.

This list contains 142 candidate members, with I -band magnitudes between 17.5 and 24. For Cha-I members within this brightness range, BT-Settl models (Allard et al. 2011) predict masses roughly between 0.002 and 0.06 M_\odot , for $A_V \leq 5^9$, and an age of 1-2 Myr. The completeness limit of the I -band catalog is 23 mag, which is equivalent to $\sim 0.003 - 0.007 M_\odot$ for $A_V \leq 5$ at 1 Myr, or $\sim 0.004 - 0.009 M_\odot$ at the age of 2 Myrs (median age of Cha-I members when compared to theoretical isochrones; Luhman 2007), and the distance of 160 pc. The completeness limit of the near-infrared catalogs is $J = 18.3$ and $Ks = 16.7$, which corresponds to masses $\sim 0.004 - 0.007 M_\odot$ for $A_V \leq 5$.

The first spectroscopic follow-up of the objects in the candidate list was performed using the multi-object spectrograph VIMOS at the VLT. The follow-up included 18 objects from the candidate list, most of which have $I < 21$. We confirmed 7 objects as VLM members of Cha-I. In the left panel of the Figure 1 we show the CMD for candidate members. For the full CMD we refer the reader to Figure 3 in Mužić et al. (2011). Two horizontal lines in the left panel mark the approximate limit of the VIMOS follow-up ($I = 21$), and the I -band completeness limit ($I = 23$). If indeed members of Cha-I, the objects between these two lines should have masses between 0.003 and 0.015 M_\odot at 1 Myr or between 0.004 and 0.02 M_\odot at 2 Myr (for $A_V \leq 5$). Red diamonds mark spectroscopically confirmed members of Cha-I, from SONYC and Luhman (2007); Luhman &

Muench (2008), while crosses mark non-members from Luhman (2004).

For the second follow-up with the Sofi/NTT, we targeted the sources with expected masses in the planetary-mass regime detected in our NIR images (the filled dots in the left panel of Figure 1, located between the two horizontal lines), and not previously observed with VIMOS (squares). The 15 Sofi follow-up targets are marked with blue triangles, and listed in Table 2.

2.2. Lupus 3

The SONYC photometric survey in Lupus 3 covers 1.4 deg^2 of the main cluster core, surrounding the two brightest members HR5999/6000. Previous surveys by Comerón et al. (2009) and Merín et al. (2008) cover approximately this same area, plus the lower-density part of the complex to the North-East of the main core. This part, however, contains only about 10% of all the candidate members identified in the two aforementioned works. The original list of photometric candidates in Lupus 3 presented in Mužić et al. (2014) was selected from the $(i - J, i)$ CMD, and contained 409 candidates. Although in our catalogs we removed the sources too close to the edges of the chips, and overly elongated or blended sources (based on SExtractor output), some extended sources (galaxies with almost round profiles, unrecognized doubles) and a few artifacts (source sitting right on a bad column, or a spike of a nearby bright object) still made it to our candidate catalog. Total of 37 contaminants of this type were found by visual inspection of the images, and have been removed from the candidate list. The final candidate list then contains 372 sources. This list can be further narrowed-down to 58, taking into account the proper motions (see Mužić et al.

⁹ According to the extinction maps of Cambrésy (1999), only about 1% of the Cha-I area has $A_V \geq 5$, while the entire Lupus 3 area appears to have $A_V < 5$. We therefore use this as an upper value of extinction when deriving mass limits from the photometry.

2014 for details). As in the previous paper, we refer to this list as the “IJ-pm” candidate list. The photometric completeness limit of our catalog is $i=20.3$, equivalent to $0.008 - 0.02 M_{\odot}$ for $A_V = 0 - 5$ at a distance of 200 pc and age of 1 Myr, according to the BT-Settl models. The magnitude range of the candidate list $I = 15.3 - 21$ is equivalent to masses $0.2 - 0.007 M_{\odot}$ for $A_V \leq 5$.

In Mužić et al. (2014), we presented the first spectroscopic follow-up using VIMOS/VLT, where we took spectra of 123 photometric candidates, out of which 32 are from the “IJ-pm” list. Spectra confirmed 7 of these objects as young members of Lupus 3, all belonging to the “IJ-pm” list. For the second follow-up, the SofI spectroscopy presented here, the targets were selected from the “IJ-pm” list not covered by the VIMOS follow-up, and above the completeness limit. The second follow-up includes 19 candidates, listed in Table 2.

The right panel of the Figure 1 shows the CMD containing 372 candidate members of Lupus 3 (dots). The proper motion candidates (“IJ-pm”) are additionally marked with open circles. Spectroscopic targets from the two follow-ups (VIMOS and SofI) are marked with black squares and blue triangles, respectively.

2.3. Spectroscopy with SofI/NTT

The spectra were taken using SofI (Son of ISAAC; Moorwood et al. 1998) at the ESO’s New Technology Telescope (NTT) during four nights in April 2014, under the program number 093.C-0050(A). SofI is equipped with a Hawaii HgCdTe 1024×1024 detector, with the pixel size projected onto the sky of $0.288''$. We used the low resolution red grism (GR Grism Red) covering the wavelength range $1.5 - 2.5 \mu\text{m}$, and delivering spectral resolution $R \sim 600$ when combined with the $1''$ slit (31 spectra), and 300 with the $2''$ slit (3 spectra). The seeing during the SofI observations was varying between 0.7 and $1.5''$ (values from the Differential Image Motion Monitor; DIMM), and the transparency was clear, except for the first few hours of the night 2014-04-17, when some clouds have been present. The wider slit was used for the particularly faint sources ($K \sim 16$), during less favorable seeing conditions. The typical nod throw along the slit was $60''$. The complete SofI target list, along with the information about the date of observation, on-source integration time, and slit used, is presented in Table 2.

Data reduction was performed by combining the SOFI pipeline recipes, our IDL routines, and IRAF task *apall*. The data reduction steps include cross-talk, flat field, and distortion corrections. Pairs of frames at different nodding positions were subtracted one from another, shifted, and combined into a final frame. The spectra were extracted using the IRAF task *apall*, and wavelength calibrated with the help of the Xenon lamp arcs. The wavelength solution obtained by the pipeline has an RMS error of $\sim 20 \text{ \AA}$. The spectra of telluric standard stars were reduced in the same way as science frames. Telluric standards spectral types range between B5V and B9.5V, and show several prominent hydrogen lines in absorption, which were removed from the spectra by interpolation, prior to division with the black body spectrum at an appropriate effective temperature. This yields the response function of the spectrograph, convolved with the telluric spectrum. Finally, we divided the science spectra by the corresponding response function. The error of the re-

sponse function is the combination of the errors of the measured telluric spectra and the errors in the effective temperature assigned to certain spectral types. The latter is caused by assumption that the intrinsic spectrum of the calibrating star is well described by a black body of a certain temperature. The error of the measured telluric spectra is supplied by *apall*, through the *extras* keyword. It is of the order, or below 1% across most of the spectrum, except in the region between H and K-bands where the atmosphere absorbs most of the light. For the B-type telluric standards, we adopted the temperature scale from Boehm-Vitense (1981), whose $\pm 5\%$ error on the effective temperature translates to approximately $\pm 1\%$ error in the response curve.

3. DATA ANALYSIS

The analysis of the spectra presented in this section consists of: (1) visual inspection of the spectra in search for the features revealing the youth, (2) fitting of the model spectra to the observed ones to determine the effective temperature and extinction, and (3) determination of spectral types.

3.1. Membership assessment

The initial assessment of the spectra is done by visual inspection. Spectra of young objects later than $\sim M5$ show a characteristic triangular peak in the H-band, caused by water absorption (Lucas et al. 2001; Cushing et al. 2005). The depth of this feature strongly depends on effective temperature, while the shape is affected by the gravity. The peak appears triangular for young, low- to intermediate-gravity¹⁰ objects, and round at higher gravities. The K-band spectra of late type objects show prominent CO absorption bands. CO bands can facilitate spectral classification, since K and M-type giants show deeper CO absorption than dwarfs (see e.g. Rayner et al. 2009). We also look for the emission lines, which may indicate accretion. Only three objects from the SofI spectroscopic sample (1 in Cha-I, 2 in Lupus 3) clearly show a triangular H-band peak. They are shown in Table 3, and Figure 2 (black), along with the corresponding best fit models (red; see the next section). SONYC-Lup3-29 is a new, probably sub-stellar member of Lupus 3. The membership is further confirmed by the mid-infrared excess, as demonstrated in Figure 3.

In Figure 2, we also show the spectrum of ISO-ChaI-192, whose steep spectrum with prominent H_2 emission lines indicates a YSO nature¹¹. Indeed, this object is a known class I protostar and an FU Ori candidate (Gramajo et al. 2014; Cambresy et al. 1998; Persi et al. 1999), associated with a CO outflow (Mattila et al. 1989; Persi et al. 2007). Gómez & Mardones (2003) derive spectral type of M3.5-M6.5 from the near infrared low-resolution spectra. Two estimates for the effective temperature are found in the literature, 3600 K by Persi et al. (2007), and 5000 K by Gramajo et al. (2014). The typical class-I SED of ISO-ChaI-192 is shown in Figure 3.

The four probable members and their properties derived in the next sections are listed in Table 3. The re-

¹⁰ $\lesssim 300$ Myr according to Allers & Liu (2013).

¹¹ The clearly detected H_2 lines are 1-0 S(2) at $2.034 \mu\text{m}$, 1-0 S(1) at $2.122 \mu\text{m}$, 1-0 S(3) at $1.957 \mu\text{m}$, 1-0 S(0) at $2.222 \mu\text{m}$, 2-1 S(1) at $2.247 \mu\text{m}$, 1-0 Q(1) at $2.404 \mu\text{m}$, 1-0 Q(3) at $2.421 \mu\text{m}$, and 1-0 Q(4) at $2.435 \mu\text{m}$.

TABLE 2
PHOTOMETRIC CANDIDATES INCLUDED IN THE SPECTROSCOPIC FOLLOW-UP WITH SOFI

#	α (J2000)	δ (J2000)	Date	Exp. time	Slit	I^a	J	K	comments
Chamaeleon-I									
1	11 05 21.36	-77 46 33.0	2014-04-19	14 × 180 s	1''	21.92	17.37	14.65	
2	11 06 18.62	-77 35 17.4	2014-04-18	12 × 180 s	1''	22.43	16.70	13.22	
3	11 06 28.04	-77 35 54.7	2014-04-13	14 × 60 s	1''	21.68	16.50	13.31	
4	11 08 20.20	-77 45 48.6	2014-04-13	10 × 200 s	1''	21.50	18.09	15.86	
5	11 08 23.59	-77 31 29.5	2014-04-14	52 × 100 s	2''	22.26	18.65	16.49	
6	11 08 30.31	-77 31 38.6	2014-04-14	52 × 100 s	2''	22.50	17.92	16.05	confirmed member
7	11 08 30.77	-77 45 50.5	2014-04-13	10 × 200 s	1''	21.34	17.77	15.59	
8	11 08 33.92	-77 46 33.4	2014-04-13	14 × 220 s	1''	21.49	18.54	16.68	
9	11 08 50.38	-77 45 53.0	2014-04-13	14 × 220 s	1''	21.26	17.90	16.01	
10	11 09 11.62	-77 19 26.1	2014-04-18	10 × 180 s	1''	21.74	16.56	13.20	
11	11 09 28.57	-76 33 28.1	2014-04-14	18 × 90 s	1''	21.95	16.74	11.93	confirmed member
12	11 09 32.26	-76 34 39.3	2014-04-19	20 × 90 s	2''	22.76	18.52	15.74	
13	11 09 35.44	-77 17 27.1	2014-04-18	8 × 180 s	1''	21.68	16.73	13.60	
14	11 09 37.38	-76 41 05.7	2014-04-17	16 × 250 s	1''	22.71	17.92	15.18	
15	11 09 51.82	-76 42 18.2	2014-04-19	12 × 180 s	1''	22.97	17.93	14.57	
Lupus 3									
16	16 08 03.96	-39 10 28.9	2014-04-18	10 × 150 s	1''	19.39	16.28	14.21	
17	16 08 25.87	-39 10 08.0	2014-04-17	8 × 120 s	1''	18.13	15.26	13.03	
18	16 08 30.04	-39 10 01.4	2014-04-17	8 × 120 s	1''	15.51	12.69	10.82	
19	16 08 33.04	-38 52 22.7	2014-04-18	6 × 180 s	1''	15.34	12.98	11.74	confirmed member
20	16 09 42.66	-39 03 20.7	2014-04-18	10 × 180 s	1''	18.68	15.54	13.29	
21	16 09 43.74	-39 07 11.9	2014-04-17	12 × 120 s	1''	18.96	15.74	13.23	
22	16 09 47.20	-39 08 42.4	2014-04-19	6 × 180 s	1''	18.92	15.91	13.82	
23	16 09 52.68	-39 06 40.4	2014-04-17	8 × 120 s	1''	17.13	14.45	12.52	
24	16 10 01.33	-39 06 45.1	2014-04-17	8 × 60 s	1''	15.38	12.32	10.52	confirmed member
25	16 10 05.97	-39 08 06.2	2014-04-18	10 × 180 s	1''	18.40	15.54	13.29	
26	16 10 06.01	-39 04 23.7	2014-04-17	6 × 60 s	1''	16.90	12.30	9.59	giant?
27	16 10 11.71	-39 09 19.8	2014-04-17	8 × 180 s	1''	17.81	14.84	12.96	
28	16 10 13.74	-39 02 34.8	2014-04-17	10 × 120 s	1''	17.21	13.49	10.86	giant?
29	16 10 14.59	-39 02 31.4	2014-04-17	10 × 120 s	1''	19.41	15.89	13.58	
30	16 10 17.86	-39 03 47.1	2014-04-17	6 × 120 s	1''	16.26	13.73	11.93	
31	16 10 30.82	-39 04 04.4	2014-04-18	6 × 180 s	1''	17.29	14.66	12.81	
32	16 10 33.59	-39 08 21.4	2014-04-17	6 × 180 s	1''	17.56	14.84	12.54	
33	16 11 46.57	-39 06 04.7	2014-04-17	8 × 90 s	1''	15.39	13.19	11.23	member?
34	16 12 04.95	-39 06 25.6	2014-04-17	6 × 120 s	1''	15.40	13.12	11.51	giant or member

^a Cousins I for sources in Chamaeleon, and DENIS i for those in Lupus

maining objects show flat spectra with few features, and cannot be easily classified at the resolution and signal-to-noise of our spectra. They are shown in Figures 4 and 5, for Lupus 3, and Cha-I, respectively, and listed in Table 2 (all objects in this table except those with the comment “confirmed member”). The fact that their spectra do not show the water absorption in the H-band indicative of cool spectral types means that they must have spectral type earlier than \sim M5, i.e. they are certainly not substellar. The lack of CO bands at $2.3\mu\text{m}$ in most of these spectra is another signpost of warm atmospheres. Only the top-most four spectra of the right panel in Figure 4 clearly show CO absorption bands. Comparison with the giant and dwarfs spectra from the IRTF spectral library (Rayner et al. 2009), reveal that they are most probably K-type giant stars, although in the case of #33 (16114657-3906047) and #34 (16120495-3906256) we cannot with certainty exclude that they are young, since the CO bands are not as deep as in the other two objects. Additionally, #33 exhibits Br γ in emission, i.e. this object might be a stellar member of Lupus 3. For the remaining objects listed in Table 2 without any comment, the low resolution and S/N of our spectra prevents a straightforward classification.

3.2. Model fitting

To determine the effective temperature and extinction of the three objects showing the prominent H-band peak, we fitted the spectra with the BT-Settl models (Allard et al. 2011). The procedure is identical to the one applied in other papers of the SONYC series using NIR spectroscopy (for a detailed description of the procedure, see Scholz et al. 2012b). The best fit solution is searched on a grid of T_{eff} varied between 2000 and 4000 K in steps of 100 K, and A_V within ± 5 mag of the value derived from photometry, by assuming the intrinsic $(J - K)_0 = 1$, and extinction law from Cardelli et al. (1989)¹². The log g is kept at a single value of 3.5, suitable for young objects that are still contracting. For the two objects in Lupus 3 no, or a very small adjustment to the photometric value of extinction ($\Delta A_V < 1$) is needed to produce a satisfying fit. For SONYC-ChaI-1, on the other hand, the value about 2 – 2.5 mag lower provides a much better solution. For the uncertainties of the fitting pro-

¹² As argued in Scholz et al. (2009), the value $(J - K)_0 = 1$ is appropriate for objects of the M spectral type. This is in agreement with values for 5-30 Myr old M-dwarfs by Pecaut & Mamajek (2013).

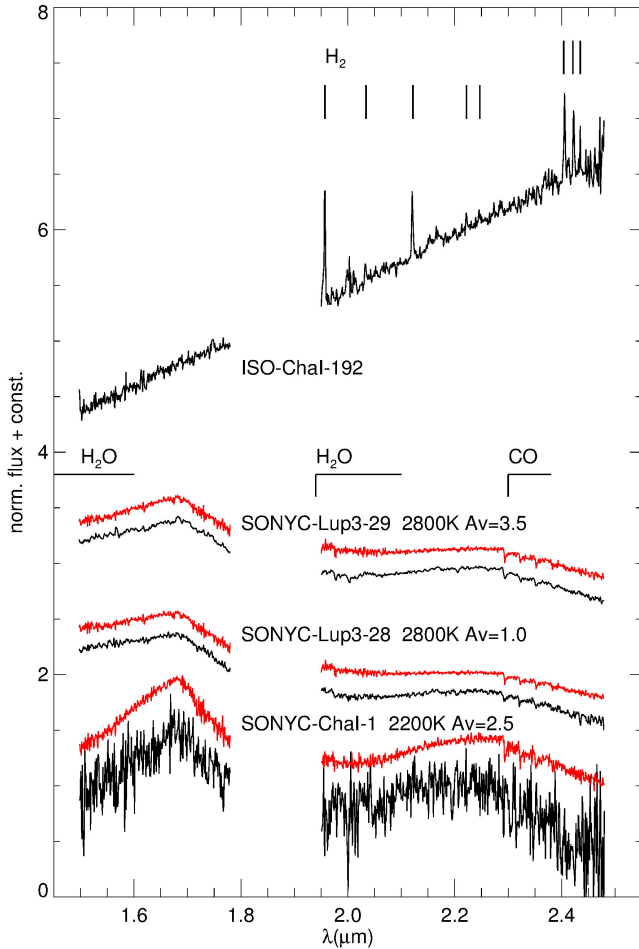


FIG. 2.— Spectra of the confirmed members of Cha-I and Lupus 3 (black), along with the BT-Settl best-fit models shown in red. All the spectra are normalized at $1.6\mu\text{m}$, and shifted by arbitrary offsets for clarity. The object spectra are as observed, and the models have been artificially reddened. The region strongly affected by telluric absorption ($1.8 - 1.95\mu\text{m}$) is not shown for clarity. The prominent molecular absorption bands observed in ultracool objects are marked. The lines marked at the top of the plot are the H_2 ro-vibrational transitions.

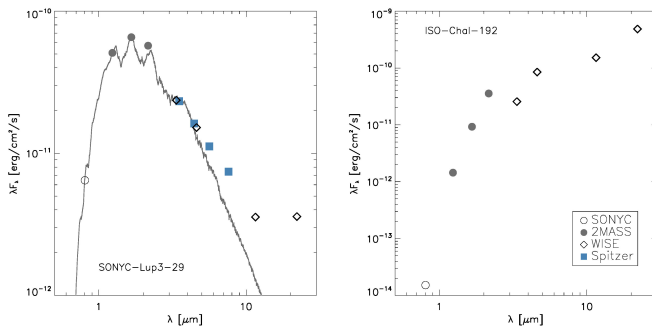


FIG. 3.— Spectral energy distribution for two objects from our follow-up showing infrared excess. The solid line in the left panel is a BT-Settl atmospheric model for a low-gravity object with $T_{\text{eff}} = 2800\text{ K}$.

cedure, we adopt the conservative values of $\pm 200\text{ K}$ for the T_{eff} , and $\pm 1\text{ mag}$ for the A_V , same as in our earlier works. SONYC-Lup3-28 was previously confirmed as a probable substellar member of Lupus 3 by Comerón et al. (2013), who derived the $T_{\text{eff}} = 2800\text{ K}$, in agreement with the value derived here. SONYC-ChaI-1 was previously reported by Luhman (2007), and classified as a probable member of Cha-I, with spectral type $\geq \text{M9}$, and $T_{\text{eff}} \leq 2400\text{ K}$, in agreement with our results.

3.3. Spectral types

We derived spectral types for the three late type members confirmed in this work, using the following spectral indices: (1) H-peak index (HPI, Scholz et al. 2012b), (2) H_2O index (Allers et al. 2007), and (3) Q-index (Willing et al. 1999). The three indices give consistent NIR spectral types for the two M-dwarfs found in Lupus 3. For SONYC-Lup3-28 we get M8 (HPI and Q-index), and M7 (H_2O), in agreement with M7.5 derived by Comerón et al. (2013). For SONYC-Lup3-29 we get M8 (HPI), M6 (H_2O), and M7 (Q). For SONYC-ChaI-1, the indices result in L2 (H_2O), and L4 (HPI and Q-index). While all the three indices are defined for young BDs earlier than L0, Scholz et al. (2012b) note that HPI might hold also at later spectral types. Allers et al. (2007) derived two SpT- H_2O index relations, one for young BDs in the M5 – L0 range, and other for the field dwarfs in M5 – L5 SpT range. They note that the two relations appear very similar, and thus the SpT-index relation can also be used for the young BDs later than L0. Luhman (2007) derive spectral type $\geq \text{M9}$ for SONYC-ChaI-1.

Prior to the calculation of the spectral types, the spectra had to be corrected for extinction. To determine the influence of extinction on the resulting spectral types, we varied the A_V derived in the previous section by $\pm 1\text{ mag}$. For HPI, we obtain the uncertainty of ± 0.3 subtypes for SONYC-Lup3-28 and -29, and ± 0.5 for the noisier SONYC-ChaI-1. For H_2O index, we get ± 0.3 for all three objects, while the Q-index does not depend on the extinction. Additionally, the uncertainties for the spectral types derived from the three indices from their respective defining papers are ± 0.4 for HPI, ± 1.0 for the H_2O -index, and ± 1.5 for the Q-index. These uncertainties have been added in quadrature to the uncertainties from the extinction, and taken into account for the calculation of the final spectral types, which were rounded-up to the nearest half-spectral type.

In Figure 6, we show a comparison of the SONYC-ChaI-1 spectrum with the spectra of field ultracool dwarfs from Allers & Liu (2013), and with the young L-type members in Upper Sco and $\rho\text{ Oph}$. Allers & Liu (2013) presented a spectroscopic study of field ultracool dwarfs having spectroscopic and/or kinematic evidence of youth ($\approx 10 - 300\text{ Myr}$). The objects are divided in three gravity classes based on the shape and strength of various features in their spectra. Three L3 objects exhibiting high-, intermediate-, and very-low gravity features are shown in the left panel of Figure 6. At the top of the same panel we also show a very-low gravity L4 object to facilitate the comparison with the young members of star forming regions, shown in the right panel. There are no suitable intermediate-gravity L4 standards presented in Allers & Liu (2013). From the shape of the H-band peak, it is evident that SONYC-ChaI-1 cannot be a

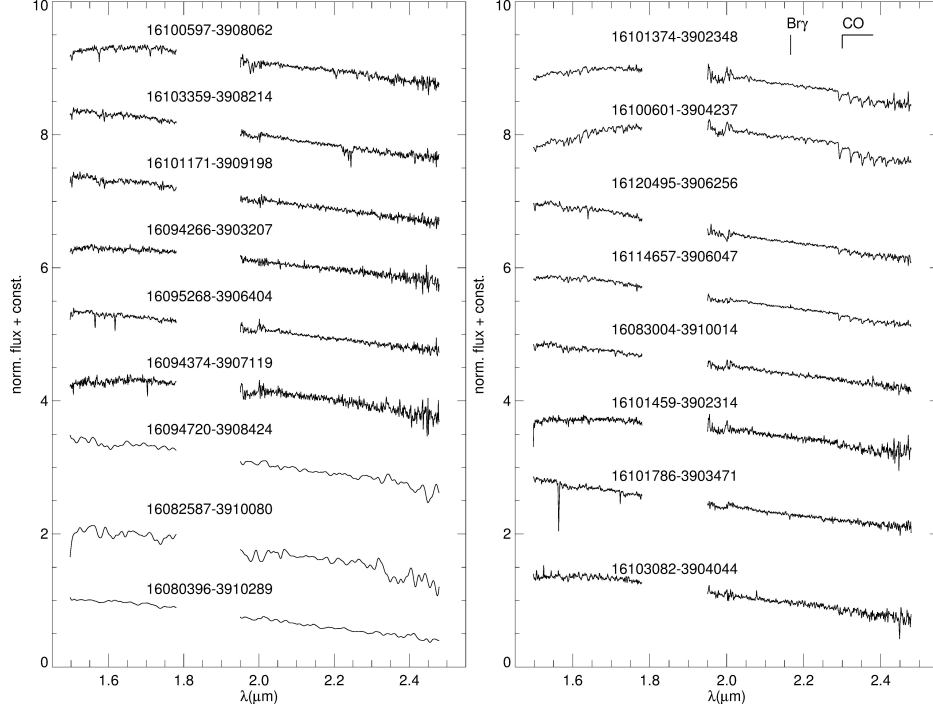


FIG. 4.— Observed spectra of candidate objects in the direction of Lupus 3, for which the membership cannot be determined with certainty. While it is clear that none of these objects is a young substellar member, it cannot be excluded that some of these still could be stellar members with spectral types earlier than $\sim M5$. All the spectra are normalized at $1.6\mu\text{m}$, and shifted by arbitrary offsets for clarity. Three spectra shown at the bottom of the left panel have lower S/N and were smoothed to better appreciate the overall broad shape of the spectra. The region strongly affected by telluric absorption ($1.8 - 1.95\mu\text{m}$) is not shown for clarity.

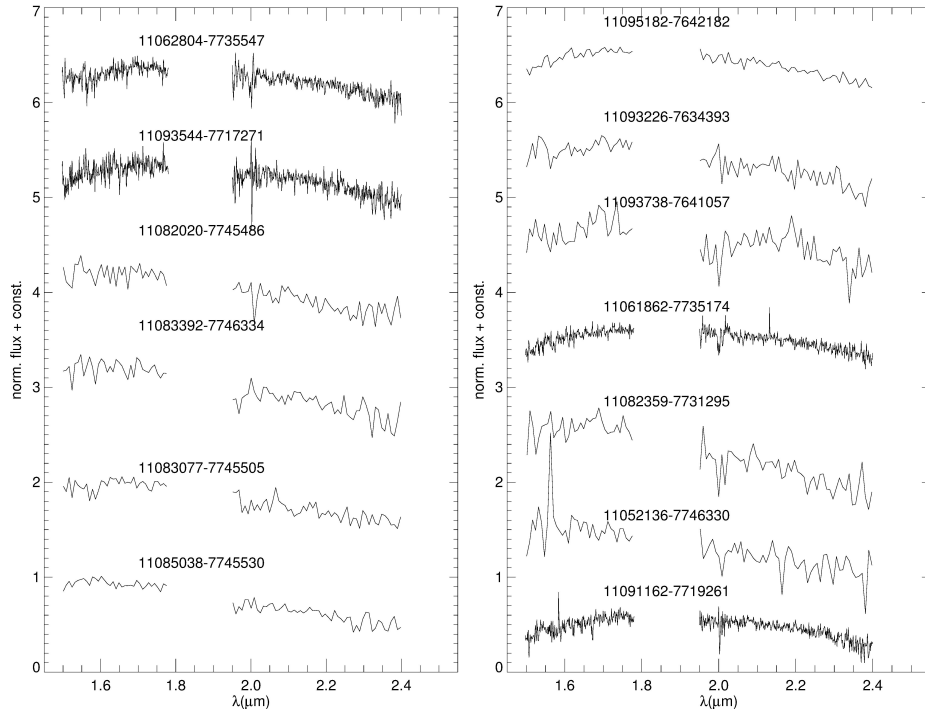


FIG. 5.— Observed spectra of candidate objects in the direction of Cha-I, for which the membership cannot be determined with certainty. While it is clear that none of these objects is a young substellar member, it cannot be excluded that some of these still could be stellar members with spectral types earlier than $\sim M5$. All the spectra are normalized at $1.6\mu\text{m}$, and shifted by arbitrary offsets for clarity. With four exceptions, the spectra were smoothed to a lower resolution to suppress the noise. The region strongly affected by telluric absorption ($1.8 - 1.95\mu\text{m}$) is not shown for clarity.

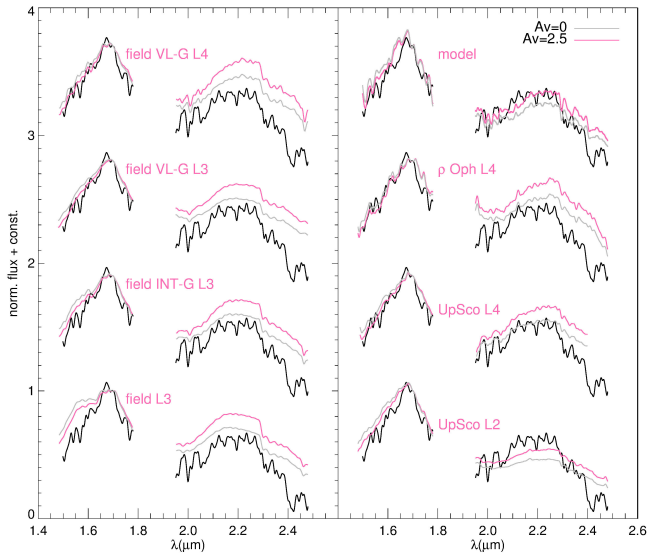


FIG. 6.— Comparison of the spectrum of SONYC-ChaI-1 (black) with the spectra of field ultracool dwarfs from Allers & Liu (2013, left panel), and young L-type members of star forming regions (right panel). Spectra of the comparison objects are shown with no reddening (grey), and with the extinction of $A_V = 2.5$ (the value estimated for SONYC-ChaI-1 from the model fitting; magenta) applied to it. The field objects are, from bottom to top, 2MASSJ0407+1546 (L3 field gravity), 2MASSJ1726+1538 (L3 intermediate gravity), 2MASSJ1615+4953 (L3 very-low gravity), and 2MASSJ15515237+0941148 (L4 very-low gravity). The young objects include two members of Upper Sco, UScoJ160603-221930 (L2; Lodieu et al. 2008) and 1RXSJ1609-2105B (L4; Lafrenière et al. 2010), and CFHTWIR-Oph33, a member of ρ Oph (L4; Alves de Oliveira et al. 2012). For a reference, we also show the best-fit BT-Settl low-gravity model (2200 K). All spectra are smoothed to the same resolution, and normalized at $1.7\mu\text{m}$.

normal field dwarf, but it is difficult to judge whether an intermediate or a low-gravity atmosphere provides a better fit. Overall, the spectral features match well both L3 or L4 low-gravity objects, but the slopes between H and K bands are different, in the sense that our object appears bluer than any of the field templates, even without extinction.

To date, there is only a limited sample of very young L-type members of star forming regions with good quality spectra available for comparison, especially at spectral types later than L1. In the right panel of Figure 6, we show two members of the Upper Scorpius association, UScoJ160603-221930 (L2; Lodieu et al. 2008) and 1RXSJ1609-2105B (L4; Lafrenière et al. 2010), along with CFHTWIR-Oph33, an L4 member of ρ Oph (Alves de Oliveira et al. 2012). The H-band portion of the SONYC-ChaI-1 spectrum matches well the young L4 templates, but in the K-band it again appears to be more consistent with $A_V = 0$, rather than with $A_V = 2.5$, the value estimated from the spectral model fitting. For a comparison, on top of the right panel we show the best-fit BT-Settl model, which clearly prefers the higher value of the extinction.

We note that detailed spectral type comparisons at young ages can be complicated by possible excess emission from disks or accretion. As demonstrated by Dawson et al. (2014), these characteristics alter the spectra of Class II objects, which then show different normalized levels between individual NIR bands. The effect is also present in Class III object spectra, to a somewhat lesser

extent.

For now, we conclude that the spectrum of SONYC-ChaI-1 is consistent with a spectral type L3-L4, $A_V \lesssim 3$, and a low-gravity atmosphere. More high quality spectra of young L-type objects are needed in order to establish a proper NIR spectral type sequence, and to create a gravity sequence at each spectral type, in comparison to the field ultracool low-gravity dwarfs from Allers & Liu (2013).

3.4. Hertzsprung-Russell Diagram

In Figure 7, we show HR diagrams for Cha-I (left panel), and Lupus 3 (right panel). The luminosities were calculated from the J -band magnitudes corrected for extinction, distance modulus, and bolometric correction. We adopt a distance of 200 pc for Lupus 3, and 160 pc for Cha-I. Extinction was calculated from the $J-K$ colors, assuming the intrinsic colors according to spectral type of each member, as listed in Pecaut & Mamajek (2013) for young (5-30 Myr) dwarf stars. We use the extinction law from Cardelli et al. (1989), with $R_V = 4$. The bolometric correction in the J band (BC_J), for the objects with $T_{\text{eff}} > 2750$ K, is calculated from the polynomial relation between BC_J and T_{eff} derived by Pecaut & Mamajek (2013). For the objects with $T_{\text{eff}} \leq 2750$ K, where this relation is not valid, we determine the BC_J as a function of $J-K_S$ color, as derived in Schmidt et al. (2014). The former relation is valid for young (5-30 Myr) dwarfs with spectral type earlier than M6, while the latter was derived for field dwarfs with spectral types M7-L8.

The HR diagram for Lupus 3 is an updated version of the one presented in Mužić et al. (2014), where we added the two objects confirmed in this work (red diamonds), and the candidate member J16114657-3906047 (purple square). For the latter we can only infer a lower limit on the T_{eff} . Since we do not know the exact spectral type of this object, we adopt the intrinsic $J-K$ color $0.6-0.9$ (used to calculate the A_V), and J -band bolometric correction 1.5 ± 0.2 mag, both suitable for young K-type stars (Pecaut & Mamajek 2013). To construct the Cha-I HR diagram, we use the photometry, T_{eff} , and extinction from the census by Luhman (2007), add the objects from Luhman et al. (2008); Luhman & Muench (2008), and the two sources confirmed in this work (red diamonds). The typical error-bars are shown in the lower left corner of the two plots. T_{eff} estimates for Lupus 3 come from various works, and we take ± 200 K as a representative uncertainty (see Mužić et al. 2014 for details). The T_{eff} of the Cha-I members marked with crosses comes from the Luhman census, who converts spectral types to T_{eff} using the scale from Kenyon & Hartmann (1995) for the stars with spectral types earlier than M, and the one from Luhman et al. (2003) for the M-type. The latter scale was designed to be compatible with the evolutionary models of Baraffe et al. (1998). Therefore, in addition to the uncertainties in spectral types, these temperature estimates are subject to a systematic uncertainty in the temperature scale, which is difficult to predict, since it depends on various details of the models, and is probably at least ± 100 K (Luhman & Muench 2008). We therefore decide to adopt a single value of ± 200 K for all objects in the plot. Different uncertainties in luminosity for objects hotter, or cooler than 2750 K in Figure 7, result from the

TABLE 3
CONFIRMED MEMBERS OF CHA-I AND LUPUS 3, FROM THE SOFI FOLLOW-UP.

No. ^a	name	α (J2000)	δ (J2000)	SpT ^b	T_{eff} /K	A_V /mag	mass/ M_{\odot} ^c	$\log(L/L_{\odot})$	comments
6	SONYC-ChaI-1	11 08 30.31	-77 31 38.6	L3 \pm 0.5	2200	2.5	0.009-0.012	-3.44 ± 0.10	$\geq M9, \leq 2400\text{K}^d$
11	ISO-ChaI-192	11 09 28.57	-76 33 28.1	-0.11 ± 0.20	
19	SONYC-Lup3-28	16 08 33.04	-38 52 22.7	M8 \pm 0.5	2800	1.0	0.05-0.06	-1.37 ± 0.11	M7.5, 2800 K ^e
24	SONYC-Lup3-29	16 10 01.33	-39 06 45.1	M7.5 \pm 0.5	2800	3.5	0.05-0.06	-0.81 ± 0.11	IR excess

^a Same as in Table 2.

^b NIR spectral type

^c estimate based on T_{eff} and BT-Settl models at 1 Myr (Lupus3), and 2 Myr (Cha-I)

^d Luhman (2007)

^e Comerón et al. (2013)

uncertainties in BC_J that were adopted from two different works (Pecaut & Mamajek 2013; Schmidt et al. 2014). The two sources with uncertain spectral type have slightly larger $\log L$ uncertainty, as a consequence of a range of extinctions and bolometric magnitudes.

In both plots, there are sources appearing well below the main sequence formed by the cluster members. In case of Cha-I, for 7 out of the 8 sources with $T_{\text{eff}} > 3000$ K that are located below the 100 Myr isochrone, Luhman (2004, 2007) argues in favor of these sources being genuine members of Cha-I, based on mid-IR excess and/or strong emission lines. Only one of the 8 sources, OTS 32, has an uncertain membership. In Lupus 3, 3 of the underluminous objects also show presence of a disk and strong emission lines, while one of them shows strong H_{α} emission, but no mid-IR excess (Mužić et al. 2014; Comerón et al. 2003; Fernández & Comerón 2005). As discussed in Comerón et al. (2003), the underluminosity of the young members of star forming regions can be explained by the object being seen only through scattered light (edge-on disk, or embedded Class I sources), or by the accretion-modified evolution, similar to what is described in Hartmann (1998) and Baraffe et al. (2009). The examples of the detail modeling of young underluminous objects with edge-on disks can be found in e.g. Scholz et al. (2010); Huélamo et al. (2010); Petr-Gotzens et al. (2010).

In Cha-I, the sequence of the objects hotter than ~ 2700 K is following the isochrones, and is mostly confined between those marking 1 and 10 Myr. Most of the coolest objects, on the other hand, fall between 10 and 100 Myr, i.e. they appear systematically underluminous relative to theoretical isochrones. One possible culprit are the bolometric corrections used to calculate the luminosities. To calculate BC_J for these objects, we use the relation from Schmidt et al. (2014), which was derived for the field dwarfs. As summarized previously in Luhman (2012), the bolometric corrections for young L and T dwarfs are probably not the same as those for standard field dwarfs, which may lead to underestimated luminosities for the young dwarfs. The bolometric corrections appropriate for the young late M and L dwarfs are not yet available, but a few individual values do exist in the literature. For example, Zapatero Osorio et al. (2010) derive $BC_J = 1.16 \pm 0.10$ for a young L3 dwarf G196-3B, whereas a field dwarf of the same spectral type would have $BC_J = 1.85 \pm 0.14$ (Schmidt et al. 2014). This difference in BC_J shifts an object by ~ 0.3 dex in the positive y-direction, i.e. enough to fall above the 10 Myr isochrone. On the other hand, Bar-

man et al. (2011a,b), studying two planetary-mass companions to young stars, suggest that the effect might be caused by an overestimate of the T_{eff} . They were able to reproduce the observed properties of the two objects by modeling low-gravity, cloudy atmospheres experiencing non-equilibrium chemistry, and requiring the T_{eff} that is several hundred K lower than reported earlier. Therefore, the position of the coolest objects in the HR-diagram with respect to the theoretical isochrones can reflect a problem with the bolometric luminosities and/or the atmosphere models in this T_{eff} regime. The latter is possibly due to treatment of dust in various models, as clouds start to form in the atmospheres of cool dwarfs with $T_{\text{eff}} \lesssim 2800$ K (Helling et al. 2008; Helling & Casewell 2014).

4. DISCUSSION

4.1. *Chamaeleon-I*

Based on the survey presented in this work, we can put limits on the number of VLM sources that are missing in the current census of YSOs in Cha-I. As in other works from the SONYC series, we use the success rates of our spectroscopic follow up (defined as a number of confirmed members divided by the number of the spectroscopically surveyed candidates), to estimate the expected number of members among the remaining photometric candidates. The listed uncertainties are the 95% confidence intervals (CI), calculated using the Clopper-Pearson method, which is suitable for small-number events, and returns conservative CIs compared to other methods (Gehrels 1986; Brown et al. 2001).

While until now for this estimate we always considered the entire candidate lists above the completeness limit, in case of Cha-I it might be more suitable to divide the candidate list in two, and consider the candidates with $I \leq 21$, and those with $21 < I < 23$ separately. The reason for this is the following. The candidate list with $I \leq 21$ contains 46 objects. We took 16 spectra with VIMOS, and confirmed 7 members. This gives a success rate of $7/16 = 44^{+26}_{-24}\%$ (95% CIs). Among the candidates with $21 < I < 23$ that were specifically targeted in this most recent follow-up, we took in total 17 spectra (15 with SofI and 2 with VIMOS), and confirmed only 1 probable VLM members of Cha-I (the other red diamond in Figure 1 marks ISO-ChaI-192, whose spectral type is unclear). The success rate is therefore $6^{+23}_{-6}\%$, which is significantly lower than for the candidates with $I \leq 21$. The difference cannot be caused simply by different wavelength domains used in spectroscopy (optical versus NIR), as all but one of the members confirmed

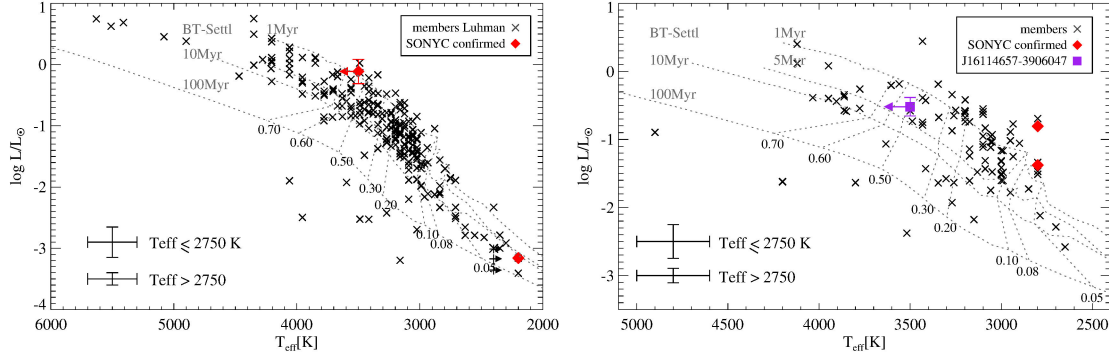


FIG. 7.— H-R diagram for Cha-I (left) and Lupus 3 (right). The crosses mark the members of ChaI from Luhman (2007); Luhman et al. (2008); Luhman & Muench (2008) and Lupus 3 from the census table in Mužić et al. (2014). Red diamonds mark the members confirmed in this work, and the purple square marks the candidate member of Lupus 3 16114657-3906047. The arrows signal the lower or upper limits on T_{eff} . The dashed lines show BT-Settl theoretical tracks for ages of 1, 5, 10, and 100 Myrs.

with VIMOS have T_{eff} below 3500 K, and would have also been recognized in the NIR.

From the success rates mentioned above, we can now estimate the number of missing VLM members in our candidate list. The number of unconfirmed members among the remaining candidates in a sample can be calculated by subtracting the number of spectra taken by SONYC and number of objects observed by other groups from the total number of candidates in the sample, multiplied by the success rate. In the higher brightness bin ($I \leq 21$), among our 46 candidates without SONYC spectra, we find additional 8 objects classified as members, and 4 non-members from Luhman (2004, 2007). Thus, the number of missing VLM objects with ($I \leq 21$) is $(46 - 16 - 8 - 4) \times 0.44^{+0.26}_{-0.24} = 8^{+5}_{-4}$. If we now consider the $21 < I < 23$ part of the Iz CMD, it contains 60 candidates, of which 17 have SONYC spectra. One probable VLM member was confirmed by SONYC, and one additional VLM was confirmed in other surveys. We estimate therefore the expected number of members in this bin to be $(60 - 17 - 1) \times 0.06^{+0.23}_{-0.06} = 3^{+10}_{-3}$. We expect most of these missing members to be substellar, although some of them might be more massive, embedded members of Cha-I.

With the above estimates in mind, we can say that the census of VLMOs in Cha-I is almost complete, down to $0.004 - 0.009 M_{\odot}$, for $A_V \leq 5$ and age of 2 Myrs.

4.2. Lupus 3

Following the discussion in the Sections 5.3 to 5.5 of Mužić et al. (2014), we can update the mass function based on the follow-up presented in this work. For this we take into account only the candidates above the completeness levels of our survey. The updated success rate in the “ IJ -pm” sample is therefore $9/50 = 18^{+13}_{-9}\%$, while for the photometric-only candidates we have $0/81 = 0^{+5}_{-0}\%$. As in the previous section, the number of unconfirmed members among the remaining candidates in a sample can be calculated by subtracting the number of spectra taken by SONYC and number of objects confirmed by other groups from the total number of candidates in the sample, multiplied by the success rate. Therefore, the estimated number of unconfirmed members in our survey is $(53 - 50) \times 0.18^{+0.13}_{-0.09} + (337 - 53 - 81 - 1) \times 0^{+0.05}_{-0} \approx 1^{+10}_{-1}$. The first term in this equation refers to the “ IJ -pm” sample, the second to other

(photometric only) candidates, and the quoted error is the 95% CI. We can repeat the same calculation to get an approximate number of missing BDs above the completeness limit, but the result is essentially the same as for all VLM objects, i.e. any of the 0 - 11 missing objects could be either stellar or substellar.

Based on these numbers, it is evident that very few potential VLM members of Lupus 3 are left to be discovered, at least down to the completeness limit of our survey, which is equivalent to $0.009 - 0.02 M_{\odot}$, for $A_V \leq 5$. Our survey covers a large portion of the entire Lupus 3 cloud, and encompasses the entire high-extinction band around the two Herbig Ae/Be members (see Figure 1 in Mužić et al. 2014) where majority of the known members are located.

Comparing Lupus 3 with Cha-I, we note that the success rate of spectroscopic confirmation of VLM candidates is significantly lower in the former, despite having used a homogenous method for selecting candidates. This can be explained by different contamination rates by background objects along the two lines of sight. The galactic longitude of Lupus 3 is $l \sim 340^\circ$, which means that we are looking towards the inner, more densely populated parts of the Galaxy, compared to regions along the line of sight to Chamaeleon ($l \sim 297^\circ$). The Besançon Milky Way stellar population synthesis model (Robin et al. 2003) yields about five times more objects in the direction of Lupus 3, than towards Cha-I, within the same area on the sky and for the same photometry limits. Lupus 3 is at the same time less populated: the current stellar census in this region contains roughly 80 members, while in Cha-I there are ~ 180 . Higher contamination by background sources, combined with a smaller overall population is therefore the most plausible cause for different success rates in our spectroscopic surveys.

4.3. Distribution of spectral types

In Figure 8 we show the distributions of spectral types for the spectroscopically confirmed VLM population in Lupus 3 (left panel), and Cha-I (right panel), found within the region covered by our surveys. The solid error bars are Poissonian confidence intervals calculated with the method described in Gehrels (1986). We do not try to correct the histograms for the missing objects estimated in the previous section, because it is not clear which spectral type they would have. Assuming that

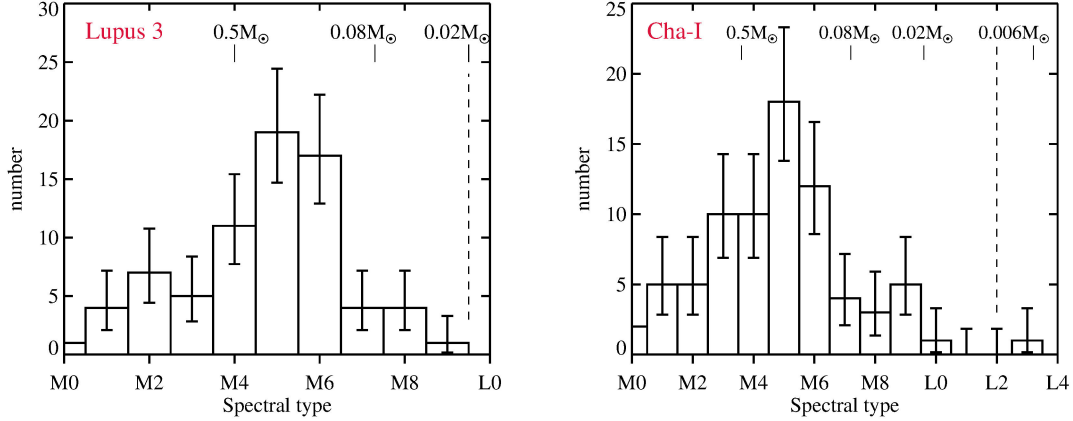


FIG. 8.— Distribution of spectral types for the VLM population of Lupus 3 (left) and Cha-I (right), within the area of our surveys. The rough mass limits according to BT-Settl isochrones are shown on top of the plot; the dashed lines mark the completeness limit of the two surveys for $A_V=5$.

they have moderate extinction ($A_V \leq 5$), we could distribute them in the substellar bins of the two histograms. However, our previous surveys have revealed a significant number of more embedded stellar members in the same part of the CMD where those moderately-extincted substellar members are found. In any case, the numbers of missing members are low, especially in Lupus 3, and they cannot strongly affect the spectral type distribution.

The overall trend seen in the two histograms is very similar, with a rise in the number of objects at spectral types earlier than M5, a peak at M5, and a drop in the number of objects at later spectral types. A similar behaviour is observed in other star forming regions, e.g. IC 348 (Luhman 2007), ρ Oph (Alves de Oliveira et al. 2012), and NGC 1333 (Scholz et al. 2012a)¹³. The sharp drop in the number of objects at spectral types M7 and later is seen in all these distributions, and is certainly a real feature of the IMF, and cannot be attributed to the incompleteness of each survey, especially in Cha-I where we are complete down to \sim L3. The survey in Lupus 3 is somewhat shallower, but from the analysis in Section 4.2 it is evident that there are very few new members left to be discovered in this region down to \sim L0. Even if we assume that all the objects missed by our surveys are substellar (i.e. in the bins M7 and later), the drop at late spectral types would remain. The two deepest SONYC surveys, in NGC 1333 and Cha-I, both contain very few objects later than M9. The two surveys are both complete down to \sim 0.005M_⊙, and reveal that the free-floating objects below D-burning limit are rare. This will be further discussed in the Section 4.6.

4.4. Star/BD ratio

To assess the numbers of stars and BDs, we use the approach described in Scholz et al. (2013). In short, by comparing the multi-band photometry¹⁴ with the predictions of the BT-Settl evolutionary models, we derive best-fit mass and A_V for each object, for the assumed distance of 160 pc and age of 2 Myr for Cha-I, and 200 pc and 1 Myr for Lupus 3, and the extinction law from

¹³ See Figure 13 in Muzić et al. (2014) for a direct comparison.

¹⁴ *IJHK* photometry complemented with the optical *BVR* bands where available from public catalogs.

TABLE 4
STAR/BD NUMBER RATIO

Chamaeleon-I			
stars	BDs	R_1^a	R_2^b
all	all	2.4 – 3.8	1.7 – 2.8
$< 1M_\odot$	all	2.0 – 3.4	1.5 – 2.5
$< 1M_\odot$	$\geq 0.03M_\odot$	3.0 – 6.1	2.5 – 5.6
Lupus 3			
stars	BDs	R_1^c	R_2^b
all	all	2.3 – 3.4	2.0 – 3.0
$< 1M_\odot$	all	1.7 – 2.7	1.6 – 2.5
$< 1M_\odot$	$\geq 0.03M_\odot$	3.0 – 6.1	2.9 – 5.8

^a in the area covered by the Luhman census

^b in the area of our survey

^c in the area covered by surveys of Merín et al. (2008) and Comerón et al. (2009)

Cardelli et al. (1989) with $R_V = 4$.

For the stellar-substellar mass boundary, we take the value at the solar metallicity, 0.075M_⊙. All the objects with estimated masses below 0.065M_⊙ are counted as BDs, and with masses above 0.085M_⊙ as stars. The remaining objects at the border of the substellar regime are once included in the higher mass bin, and then in the lower mass bin, thus resulting in a lower and upper limit of the star/BD ratio.

In Cha-I, we take the census from Luhman (2004, 2007), and complement it with the objects identified in Luhman et al. (2008); Luhman & Muench (2008), resolved binaries from Daemgen et al. (2013), and one VLM object identified here. In Table 4, we list various star/BD number ratios, calculated for different mass bins, and for the area of the Luhman census, as well as the area encompassed by our survey. The limits on stellar mass $< 1M_\odot$, and BD mass $\geq 0.03M_\odot$ were chosen to facilitate comparison with our previous works (e.g. Scholz et al. 2013).

The stellar and substellar population of Lupus 3 has not been as thoroughly surveyed by spectroscopy in the past as that of Cha-I. If we look at only the spectroscop-

ically confirmed members, it is clear from Fig. 8 that the number of objects in the M6 bin is larger than the total number of objects in lower mass bins. Since a good fraction of the objects in the M6 bin are at the substellar border, we end up with a very large span of values for the star-to-BD ratio. However, Lupus 3 certainly has a larger fraction of candidate sources that still await a spectroscopic confirmation. For example, the work of Merín et al. (2008) contains 124 candidates, of which only 46 have been surveyed by spectroscopy. We therefore apply a slightly different approach to calculate the star-to-BD ratio in Lupus 3. We use the following (candidate) member lists: (1) census of spectroscopically confirmed M-type objects from Mužić et al. (2014), updated with the newly discovered object SONYC-Lup3-29; (2) candidates from Merín et al. (2008), excluding those already in the census table. The numbers from this sample are multiplied by the success rate of the spectroscopic follow-up (36/46; Mortier et al. 2011), and by the factor 1.25 to account for the fact that the survey is only sensitive to objects with disks, whose fraction is estimated to be 70-80%; (3) candidates from Comerón et al. (2009), excluding those already in the census table. The numbers from this sample are multiplied by 0.5, which is the success rate of the spectroscopic follow-up presented in Comerón et al. (2013); (4) known members with the spectral type earlier than M, from Comerón (2008). The results for the stars-to-BD ratio are shown in Table 4, for the area encompassed by our survey, as well as for the larger area covered by Merín et al. (2008) and Comerón et al. (2009).

The numbers listed in Table 4 for Cha-I and Lupus 3 are consistent with each other, and are also generally consistent with the star-to-BD ratios derived for NGC 1333 and IC 348 by Scholz et al. (2013). Clearly, there are a number of uncertainties involved in this calculation, such as the choice of the isochrones and extinction law used to derive masses, or uncertainties in distances to star forming regions. In Lupus 3, in particular, there could also be some effects of possible incompleteness at the overlap of the different studies.

The numbers in Table 4 do not include our estimate for the objects that are “missing” in our census. In Cha-I, where the stellar population has been thoroughly characterized by spectroscopy in the works of Luhman et al., we estimate that there might still be 11^{+11}_{-5} unidentified members in our selection box. According to the BT-Settl models, at moderate extinctions ($A_V < 5$), these objects should be substellar, although some of them might be more embedded stellar members. If these objects would be substellar, the ratio of the star-to-BD ratio R_2 could be as low as 1, with the upper limit of 2.3. In Lupus 3, where we surveyed almost entire population of the photometric and proper motion candidates, the number of missing objects is 0^{+10}_{-0} . With this upper 95% confidence limit, the star-to-BD ratio R_2 would be slightly lower: 1.7-2.4 taking into account all stars and BDs, and 1.4-1.9 if we consider only stars below $1M_\odot$.

To conclude, the star/BD ratio in Cha-I and Lupus 3 is consistent with the findings in other clusters, and we find that for each formed BD there are between 1.5 and 6 formed stars. To probe finer differences, one needs a more sophisticated analysis and better constraints on fundamental parameters.

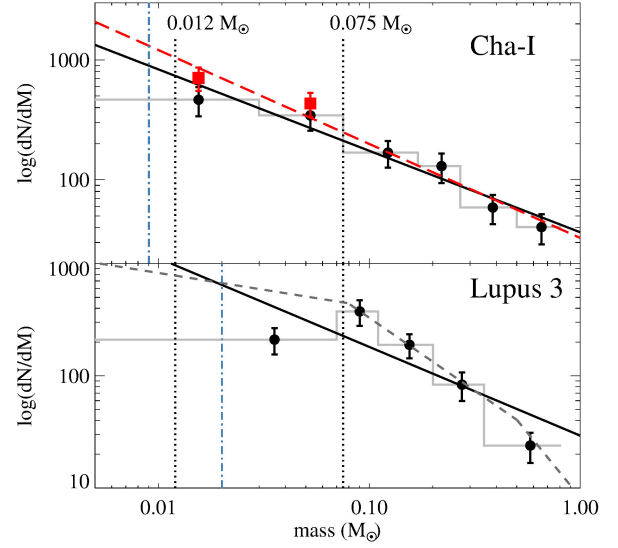


FIG. 9.— Mass spectrum for low mass stars and BDs in Cha-I (upper panel) and Lupus 3 (lower panel), within the areas of our surveys. The bin sizes were chosen to contain similar number of members. The red squares in the Cha-I plot account for the numbers of missing objects (see text). The vertical error bars represent the Poisson uncertainties. The solid black lines show the best fit to the data (black circles), and the red dashed line in the upper panel is the best-fit to the data when the red squares are used instead of the circles at their respective masses. The vertical dotted lines mark the approximate locations of H- and D-burning limits, and the dash-dotted lines represent the completeness of the two surveys at $A_V = 5$. The grey dashed line in the lower panel is the Kroupa segmented power-law mass function.

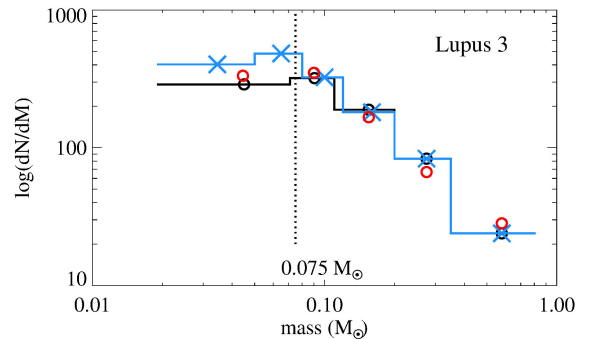


FIG. 10.— Mass spectrum in Lupus 3. Black circles and histogram show the same data as shown in the lower panel of Figure 9, only restricted to masses above $0.02M_\odot$, which is our conservative completeness limit at $A_V = 5$. Red circles show the mass spectrum for the same sample of stars, but with masses calculated after random variation of A_V (see text). Blue crosses and histogram show the mass spectrum after adding 11 substellar objects with masses above our completeness limit at $A_V=0$ ($0.009M_\odot$). The bins are modified to have similar error bars, which are not shown here for clarity, but are similar to those in Figure 9.

4.5. Initial Mass Function

With the masses calculated as described in the previous section, we can construct the IMFs in Cha-I and Lupus 3. They are shown in Figure 9, where we varied the bin size in order to achieve similar numbers of members in each bin. We choose to express the IMF in the power-law form, as $dN/dM \propto M^{-\alpha}$. The data needed

to reproduce the plot are given in Table 5. In Cha-I the best fit yields $\alpha = 0.68 \pm 0.09$ (black solid line). We can also account for the number of objects missing in our census, as estimated in Section 4.1. It is not simple to predict the masses that these “missing” objects should have, because of the variable extinction in star forming regions, where more massive embedded stellar members might mix in the color-magnitude space with the less embedded substellar members. However, if we assume the typical $A_V < 5$, then our missing members should be substellar. The objects in the $21 < I < 23$ bin were included in the lowest-mass bin ($0.001 - 0.03M_\odot$), as they are expected to have masses below $0.015M_\odot$. Objects with $17.5 < I < 21$ should have spectral type M7 - L0, and we distribute half of those in each of the two lowest-mass (substellar) bins. With this correction, the best-fit power-law index (dashed red line) becomes $\alpha = 0.78 \pm 0.08$. The slope remains essentially unchanged if we put all the missing objects with $17.5 < I < 21$ to the more massive of the two substellar bins ($0.03-0.075M_\odot$). Despite the caveat mentioned above, this short exercise tells us that even in the (somewhat extreme) case that all the missing members were substellar, the slope of the IMF would not be strongly affected.

In Lupus 3, we get the best fit single power-law index $\alpha = 0.79 \pm 0.13$ (bottom panel of Figure 9). Here the lowest-mass bin contains all the substellar objects. While in Cha-I all the data points seem to be consistent with a single power-law, in Lupus 3 there might be an indication of the flattening of the slope in the substellar regime. For a comparison, we show the segmented power-law IMF by Kroupa (2001), where the power-law slope changes at 0.5 and $0.08M_\odot$. The Kroupa IMF, normalized to match the middle point of the Lupus 3 IMF at $0.155M_\odot$, is shown by the dashed grey line in the lower panel of Figure 9, with the slopes $\alpha = 2.3$ for $M > 0.5M_\odot$, $\alpha = 1.3$ for $0.08 < M < 0.5M_\odot$, and $\alpha = 0.3$ for $M < 0.08M_\odot$. The possible turnover in the power-law mass function in the substellar regime that we observe in Lupus 3, has not been, to our best knowledge, reported in any other spectroscopically confirmed sample of a young cluster. One possible exception is the young, sparsely populated association η Cha, which beside the population of ~ 15 stars of spectral type K and M, does not contain any BDs down to $0.015M_\odot$ (Luhman & Steeghs 2004). Assuming the star-to-BD ratio of 1.5 – 6 that we find for Lupus 3 and Cha-I, one would expect a population of 3 – 10 BDs. However, a comparison of the mass distributions in η Cha, Cha-I, and IC 348 by means of a two-sided Kolmogorov-Smirnov test, does not reveal a significant difference between the three clusters (Luhman et al. 2009).

To test the significance of our findings for the Lupus 3 power-law mass function, we first add the upper limit of 11 missing members to the substellar bin. The objects have random masses above our completeness limit for $A_V=0$ ($0.009M_\odot$), and below the substellar limit. This case is extreme, both regarding the number of missing objects (the estimate from Section 4.2 was 1^{+10}_{-1}), and by the assumption that all the potentially missing members would be substellar, since some, or even all of them could equally be stellar. The result is shown in Figure 10, represented by blue crosses and histogram. After adding the missing members, the bins have been redistributed

to contain similar numbers of objects. Black circles and histogram show the spectroscopic IMF from Figure 9, restricted to masses above our conservative completeness limit at $A_V = 5$ ($0.02M_\odot$). We see that even after adding the upper limit of the possibly missing objects, the flattening of the slope remains.

A second suitable test concerns possible influence of the extinction. Here, we derived masses and A_V simultaneously by fitting the photometry to the predictions of the evolutionary models. Alternatively, we could have fixed the A_V to the value derived from spectroscopy, or from a single intrinsic color (e.g. $J - K$, as in Section 3.4). Since for the majority of the objects these values do not differ by a large amount, the resulting IMF looks unchanged. To further test the impact of the extinction value used to derive masses, we varied the A_V by a random amount in the interval ± 2 mag from the spectroscopic value. We have done this 1000 times for each object, and finally adopted the average mass from all the variations. The result is shown in Figure 10, with red open circles. We see that this has a small impact on the shape of the IMF. As mentioned earlier in the paper, members of Lupus 3 typically have low extinction ($\lesssim 5$). In fact, the spectroscopic sample used to plot the IMF contains 98% of members with $A_V \leq 3$. At $A_V = 10$, a $0.07M_\odot$ object would fall right at the completeness limit of our survey, i.e. at the extinctions above 10, we would not be able to detect substellar objects. However, we do not expect that many BD could be hiding at high extinctions, because in this case we should have also found some highly embedded stellar objects. The optical part of our spectroscopic survey would be sensitive to those, but we detect only one such source (SONYC-Lup3-1), whose spectrum and SED suggest a rare geometrical configuration (edge-on disk).

The single power-law slopes of the mass functions for the two star forming regions derived here agree well, and are also consistent with typical values found in the literature¹⁵. Scholz et al. (2012a) find $\alpha = 0.6 \pm 0.1$ for low-mass stars and BDs below $0.6M_\odot$ in NGC 1333, whereas Scholz et al. (2013), in a slightly modified analysis, report $\alpha = 0.9 - 1.0$ for the same cluster. In IC348, Alves de Oliveira et al. (2013) report α of 1.0 ± 0.3 and 0.7 ± 0.4 for the substellar ($\leq 80M_{Jup}$) IMF extinction-limited, and spatially limited to the center of the cluster, respectively. This is consistent with $\alpha = 0.7 - 0.8$ found in the same cluster by Scholz et al. (2013). Alves de Oliveira et al. (2013) also find $\alpha = 0.8 \pm 0.4$ and 0.7 ± 0.3 for the substellar regime in ρ Oph, with the extinction limited to $A_V \leq 8$, and $A_V \leq 15$, respectively. For low-mass stars and BDs in σ Ori ($0.35 - 0.006M_\odot$), Peña Ramírez et al. (2012) find $\alpha = 0.6 \pm 0.2$, in agreement with earlier works in the same region (Caballero et al. 2007; Béjar et al. 2011). In Upper Sco, assuming the age of 5-10 Myrs, Lodieu (2013); Lodieu et al. (2013a), report $\alpha = 0.5 - 0.7$, for the mass range $\sim 0.03 - 0.005M_\odot$. Zapatero Osorio et al. (2014) report α between 0 and 1 for the Pleiades cluster, down to $\approx 0.012M_\odot$.

We now outline the environmental conditions in our two clusters, to try to understand the origin of the difference between the two IMFs in the substellar regime.

¹⁵ Here we list only the most recently published results, for earlier works see Scholz et al. (2012a).

TABLE 5
VALUES FOR THE MASS FUNCTIONS SHOW
IN FIGURE 9.

Mass interval	Mean mass	dN/dM
Chamaeleon-I		
0.001 - 0.030	0.0155	465.52
0.030 - 0.075	0.0525	344.44
0.075 - 0.170	0.1225	168.42
0.170 - 0.270	0.2200	130.00
0.270 - 0.500	0.3850	58.70
0.500 - 0.810	0.6550	40.32
Lupus 3		
0.001 - 0.070	0.0355	210.15
0.070 - 0.110	0.0900	375.00
0.110 - 0.200	0.1550	188.89
0.200 - 0.350	0.2750	83.33
0.350 - 0.810	0.5800	23.91

According to Gutermuth et al. (2009), with 19 stars pc^{-2} Lupus 3 has the lowest mean surface density among nearby star forming regions, several times lower than e.g. ρ Oph (120 pc^{-2}) and NGC 1333 (65 pc^{-2}), and also lower than Serpens (36 pc^{-2}), Cha-I (30 pc^{-2}), CrA (29 pc^{-2}), or IC 348 (25 pc^{-2}). In terms of peak surface densities, Cha-I is twice as dense as Lupus 3 (800 vs 400 pc^{-2}). In Scholz et al. (2013), we presented evidence for a difference in mass distributions of NGC 1333 and IC 348, under the (plausible) assumption that NGC 1333 is closer to us. The denser of the two clusters (NGC 1333) harbors a larger fraction of BDs. Therefore, frequencies of BDs might depend on stellar densities, which is in line with predictions for BD formation through gravitational fragmentation of filaments falling into a cluster potential (Bonnell et al. 2008), dynamical cluster formation (simulations by Bate 2012), or even the disk fragmentation in some cases (see discussion in Scholz et al. 2013).

The presence of massive OB stars might influence BD formation in clusters, since BDs could form through photo-evaporation of prestellar cores (Whitworth & Zinnecker 2004). However, nearby star forming regions ($d \lesssim 300 \text{ pc}$) contain extremely small populations of OB stars (only one B star in Lupus, and three in Cha-I), and their influence on the IMF of these clusters must be negligible.

4.6. Brown dwarfs with masses below the deuterium-burning limit

If we assume monotonic continuation of the power law shown in the upper panel of Figure 9 below the D-burning limit, we would expect 8 ± 4 objects with $0.005 < M < 0.015 M_{\odot}$ in Cha-I. For the slope shown with the red dashed line, which accounts for the objects possibly missed by our follow-up, we get 12 ± 5 . Our method for mass estimates from photometry yields 6 objects with masses below $\sim 0.015 M_{\odot}$ in the area of our survey, and we estimated that there might be 3^{+10}_{-3} more in our candidate list. The data are therefore consistent with a monotonic power law mass spectrum across the D-burning limit, and down to $\sim 0.005 M_{\odot}$.

In NGC 1333, we find similar monotonic behavior of the low-mass IMF across the D-burning limit, but do not exclude a shallower slope below this limit (i.e. $\alpha \lesssim 0.6$).

In fact, based on more recent information about the mid-infrared colors of young ultracool objects (Faherty et al. 2013), our upper limit on the number of the planetary-mass BDs is probably too conservative, and is likely to be lower (4 instead of 8). This suggests a possible break in the power-law around D-burning limit. In σ Ori, Peña Ramírez et al. (2012) report the IMF consistent with a smooth power law with $\alpha = 0.6 \pm 0.2$ down to $0.004 M_{\odot}$. In the range $0.004 - 0.003 M_{\odot}$ there are fewer candidate members observed in their deep J-band catalog than one would expect from an extrapolation of the same power-law to these masses, possibly signaling a lower slope in this mass regime. Lodieu et al. (2013a) present a deep NIR survey probing the planetary-mass regime in UpSco, complementing their previous work in the same region (Lodieu 2013). The updated IMF in UpSco, extending down to $\sim 0.005 M_{\odot}$, is consistent with a rising power-law function with $\alpha \sim 0.5$.

In the area of our Cha-I survey, there are in total 94 known members, out of which ~ 6 appear to have masses below $0.015 M_{\odot}$. Previously we estimated that there might be 0-13 objects missing in this mass regime, and 4-13 among the higher mass BDs. In the current census, the brown dwarfs with masses in the planetary-mass regime seem to comprise only $\sim 6\%$ of the Cha-I population, whereas their contribution can go up to $\sim 17\%$ taking into account these estimates. Even in the extreme case, the mass budget of these objects can be only about 1% of the total mass of the cluster.

In Lupus 3, our survey is sensitive only to the high-mass tip of the planetary-mass regime, but Comerón (2011) conducted a small-area photometric survey several magnitudes deeper than ours and sensitive to free-floating Jupiters according to the models. The saturation of their survey matches the completeness limits of ours, and their 3σ detection limit is at $I_C = 25.6 \text{ mag}$. The number of the cool photometric candidates identified in the survey by Comerón (2011) is consistent with statistical expectation of a background population. The survey encompasses a very small part of Lupus 3, about 100 times smaller than the SONYC area, but carefully chosen to match an area known to be rich in higher mass stellar and substellar members. While a wider area survey sensitive to the lowest masses is still required to confirm the result by Comerón (2011), it represents a complement to our finding that there are very few substellar members left to be discovered down to the mass limits of our survey.

To conclude, surveys in various star forming regions clearly show that the IMF below $\sim 0.6 M_{\odot}$, and down to $\sim 0.02 M_{\odot}$ can be well described by a monotonic power-law with an exponent $\alpha = 0.6 - 1.0$. Below the D-burning limit, the slope seems to be similar, or shallower, but it is certainly not steeper than the one above $0.02 M_{\odot}$. This means that, if the microlensing results (Sumi et al. 2011) hold, the objects they probe must undergo a different formation path than those studied so far in young clusters.

5. CONCLUSIONS AND SUMMARY

Here we have presented the further spectroscopic follow-up of the VLM candidate member lists in Cha-I and Lupus 3, using the NIR spectrograph SofI at the NTT. This work is a continuation of our previous efforts

described in Mužić et al. (2011) and Mužić et al. (2014).

In Lupus 3, we obtained 19 new spectra of our high priority photometric and proper motion sample (“*iJ*-pm”), thus almost completing the spectroscopic survey of this sample: we have targeted 50 out of 53 candidates above the surveys completeness limit. We identified two probable substellar members of Lupus 3, one of which is new and has a NIR spectral type M7.5. Based on statistical arguments, we conclude that only a very few substellar members are left to be discovered in this region, at least down to the completeness limit of our survey, lying at $i = 20.3$, equivalent $0.008 - 0.02 M_{\odot}$, for $A_V \leq 5$ at 1 Myr.

The follow-up in Cha-I included 15 candidates with expected masses in the planetary regime, of which only one was confirmed as substellar with the spectral type L3 and T_{eff} of 2200 K. According to the BT-Settl models, an object at this T_{eff} should have a mass of $\sim 0.009 - 0.012 M_{\odot}$ at the age of 1-2 Myr. The comparison of the multi-wavelength photometry of this object with the models yields a mass of $\sim 0.007 M_{\odot}$, at the distance of Cha-I and age of 2 Myr. Based on statistical arguments, we estimate that in the area of our survey, 8_{-4}^{+5} objects are left to be discovered with $17.5 < I < 21$, and $3_{-3}^{+10}\%$ with $21 < I < 23$. In terms of masses, the first bin is equivalent $0.005 - 0.06 M_{\odot}$, and the second one $0.003 - 0.02 M_{\odot}$, at the age of 1-2 Myr, and $A_V \leq 5$.

The IMF below $1 M_{\odot}$ in both Cha-I and Lupus 3 can be described by a power law $dN/dM \propto M^{-\alpha}$, with the slope $\alpha \sim 0.7$, in agreement with the results of the surveys in other clusters. The same is valid for the star-to-BD ratio, which is found to be between 1.5 and 6. In Lupus 3, however, we find evidence for a flattening of the slope, or even a possible turnover of the IMF in the power law form in the substellar regime: this region seems to produce less BDs in comparison to majority of other clusters. The flattening is still present even after accounting for the maximum number of objects possibly missed by our survey.

The IMF in Cha-I shows a monotonic behaviour across the D-burning limit. The expected total number of substellar objects can be statistically estimated from the success rates of our spectroscopic follow-up, and this estimate yields numbers consistent with the same power law extending down to our completeness limit, lying at $0.004 - 0.009 M_{\odot}$. We estimate that the low-mass members below the D-burning limit contribute of the order 5 – 15% to the total number of Cha-I members, comprising therefore $\lesssim 1\%$ of the mass budget of the cluster.

The authors thank Katelyn Allers, Catarina Alves de Oliveira, and David Lafrenière for sharing their spectra, used for comparison in this work. This work was co-funded by NSERC grants to R.J.

REFERENCES

- Allard, F., Homeier, D., & Freytag, B. 2011, in *Astronomical Society of the Pacific Conference Series*, Vol. 448, 16th Cambridge Workshop on Cool Stars, Stellar Systems, and the Sun, ed. C. Johns-Krull, M. K. Browning, & A. A. West, 91
- Allers, K. N., Jaffe, D. T., Luhman, K. L., Liu, M. C., Wilson, J. C., Skrutskie, M. F., Nelson, M., Peterson, D. E., Smith, J. D., & Cushing, M. C. 2007, *ApJ*, 657, 511
- Allers, K. N. & Liu, M. C. 2013, *ApJ*, 772, 79
- Alves de Oliveira, C., Moraux, E., Bouvier, J., & Bouy, H. 2012, *A&A*, 539, A151
- Alves de Oliveira, C., Moraux, E., Bouvier, J., Duchêne, G., Bouy, H., Maschberger, T., & Hudelot, P. 2013, *A&A*, 549, A123
- Baraffe, I., Chabrier, G., Allard, F., & Hauschildt, P. H. 1998, *A&A*, 337, 403
- Baraffe, I., Chabrier, G., Barman, T. S., Allard, F., & Hauschildt, P. H. 2003, *A&A*, 402, 701
- Baraffe, I., Chabrier, G., & Gallardo, J. 2009, *ApJ*, 702, L27
- Barman, T. S., Macintosh, B., Konopacky, Q. M., & Marois, C. 2011a, *ApJ*, 733, 65
- . 2011b, *ApJ*, 735, L39
- Basu, S. & Vorobyov, E. I. 2012, *ApJ*, 750, 30
- Bate, M. R. 2009, *MNRAS*, 392, 590
- . 2012, *MNRAS*, 419, 3115
- Bayo, A., Barrado, D., Stauffer, J., Morales-Calderón, M., Melo, C., Huélamo, N., Bouy, H., Stelzer, B., Tamura, M., & Jayawardhana, R. 2011, *A&A*, 536, A63
- Béjar, V. J. S., Zapatero Osorio, M. R., Rebolo, R., Caballero, J. A., Barrado, D., Martín, E. L., Mundt, R., & Bailer-Jones, C. A. L. 2011, *ApJ*, 743, 64
- Boehm-Vitense, E. 1981, *ARA&A*, 19, 295
- Bonnell, I. A., Clark, P., & Bate, M. R. 2008, *MNRAS*, 389, 1556
- Brown, L. D., Cai, T. T., & Dasgupta, A. 2001, *Statistical Science*, 16, 101
- Caballero, J. A., Béjar, V. J. S., Rebolo, R., Eisloffel, J., Zapatero Osorio, M. R., Mundt, R., Barrado Y Navascués, D., Bihain, G., Bailer-Jones, C. A. L., Forveille, T., & Martín, E. L. 2007, *A&A*, 470, 903
- Cambresy, L. 1999, *A&A*, 345, 965
- Cambresy, L., Copet, E., Epchtein, N., de Batz, B., Borsenberger, J., Fouque, P., Kimeswenger, S., & Tiphene, D. 1998, *A&A*, 338, 977
- Cardelli, J. A., Clayton, G. C., & Mathis, J. S. 1989, *ApJ*, 345, 245
- Chabrier, G., Baraffe, I., Allard, F., & Hauschildt, P. 2000, *ApJ*, 542, 464
- Comerón, F. 2008, *The Lupus Clouds*, ed. B. Reipurth, 295
- . 2011, *A&A*, 531, A33
- Comerón, F., Fernández, M., Baraffe, I., Neuhäuser, R., & Kaas, A. A. 2003, *A&A*, 406, 1001
- Comerón, F., Spezzi, L., & López Martí, B. 2009, *A&A*, 500, 1045
- Comerón, F., Spezzi, L., López Martí, B., & Merín, B. 2013, *A&A*, 554, A86
- Cushing, M. C., Rayner, J. T., & Vacca, W. D. 2005, *ApJ*, 623, 1115
- Daemgen, S., Petr-Gotzens, M. G., Correia, S., Teixeira, P. S., Brandner, W., Kley, W., & Zinnecker, H. 2013, *A&A*, 554, A43
- Dawson, P., Scholz, A., Ray, T. P., Peterson, D. E., Rodgers-Lee, D., & Geers, V. 2014, *MNRAS*, 442, 1586
- Faherty, J. K., Rice, E. L., Cruz, K. L., Mamajek, E. E., & Núñez, A. 2013, *AJ*, 145, 2
- Fernández, M. & Comerón, F. 2005, *A&A*, 440, 1119
- Gehrels, N. 1986, *ApJ*, 303, 336
- Gómez, M. & Mardones, D. 2003, *AJ*, 125, 2134
- Gramajo, L. V., Rodón, J. A., & Gómez, M. 2014, *AJ*, 147, 140
- Gutermuth, R. A., Megeath, S. T., Myers, P. C., Allen, L. E., Pipher, J. L., & Fazio, G. G. 2009, *ApJS*, 184, 18
- Hartmann, L. 1998, *Accretion Processes in Star Formation*
- Helling, C., Ackerman, A., Allard, F., Dehn, M., Hauschildt, P., Homeier, D., Lodders, K., Marley, M., Rietmeijer, F., Tsuji, T., & Woitke, P. 2008, *MNRAS*, 391, 1854
- Helling, C. & Casewell, S. 2014, *A&A Rev.*, 22, 80
- Huélamo, N., Bouy, H., Pinte, C., Ménard, F., Duchêne, G., Comerón, F., Fernández, M., Barrado, D., Bayo, A., de Gregorio-Monsalvo, I., & Olofsson, J. 2010, *A&A*, 523, A42
- Ingraham, P., Albert, L., Doyon, R., & Artigau, E. 2014, *ApJ*, 782, 8
- Kenyon, S. J. & Hartmann, L. 1995, *ApJS*, 101, 117
- Kroupa, P. 2001, *MNRAS*, 322, 231

- Lafrenière, D., Jayawardhana, R., & van Kerkwijk, M. H. 2010, *ApJ*, 719, 497
- Lodieu, N. 2013, *MNRAS*, 431, 3222
- Lodieu, N., Dobbie, P. D., Cross, N. J. G., Hambly, N. C., Read, M. A., Blake, R. P., & Floyd, D. J. E. 2013a, *MNRAS*, 435, 2474
- Lodieu, N., Hambly, N. C., Dobbie, P. D., Cross, N. J. G., Christensen, L., Martin, E. L., & Valdivielso, L. 2011, *MNRAS*, 418, 2604
- Lodieu, N., Hambly, N. C., Jameson, R. F., & Hodgkin, S. T. 2008, *MNRAS*, 383, 1385
- Lodieu, N., Ivanov, V. D., & Dobbie, P. D. 2013b, *MNRAS*, 430, 1784
- Lucas, P. W., Roche, P. F., Allard, F., & Hauschildt, P. H. 2001, *MNRAS*, 326, 695
- Luhman, K. L. 2004, *ApJ*, 602, 816
- . 2007, *ApJS*, 173, 104
- . 2012, *ARA&A*, 50, 65
- Luhman, K. L., Allen, L. E., Allen, P. R., Gutermuth, R. A., Hartmann, L., Mamajek, E. E., Megeath, S. T., Myers, P. C., & Fazio, G. G. 2008, *ApJ*, 675, 1375
- Luhman, K. L., Mamajek, E. E., Allen, P. R., & Cruz, K. L. 2009, *ApJ*, 703, 399
- Luhman, K. L. & Muench, A. A. 2008, *ApJ*, 684, 654
- Luhman, K. L., Stauffer, J. R., Muench, A. A., Rieke, G. H., Lada, E. A., Bouvier, J., & Lada, C. J. 2003, *ApJ*, 593, 1093
- Luhman, K. L. & Steeghs, D. 2004, *ApJ*, 609, 917
- Mattila, K., Liljeström, T., & Toriseva, M. 1989, in *European Southern Observatory Conference and Workshop Proceedings*, Vol. 33, *European Southern Observatory Conference and Workshop Proceedings*, ed. B. Reipurth, 153–171
- Merín, B., Jørgensen, J., Spezzi, L., Alcalá, J. M., Evans, II, N. J., Harvey, P. M., Prusti, T., Chapman, N., Huard, T., van Dishoeck, E. F., & Comerón, F. 2008, *ApJS*, 177, 551
- Moorwood, A., Cuby, J.-G., & Lidman, C. 1998, *The Messenger*, 91, 9
- Mortier, A., Oliveira, I., & van Dishoeck, E. F. 2011, *MNRAS*, 418, 1194
- Mužić, K., Scholz, A., Geers, V., Fissel, L., & Jayawardhana, R. 2011, *ApJ*, 732, 86
- Mužić, K., Scholz, A., Geers, V. C., Jayawardhana, R., & López Martí, B. 2014, *ApJ*, 785, 159
- Offner, S. S. R., Clark, P. C., Hennebelle, P., Bastian, N., Bate, M. R., Hopkins, P. F., Moraux, E., & Whitworth, A. P. 2014, *Protostars and Planets VI*, 53
- Peña Ramírez, K., Béjar, V. J. S., Zapatero Osorio, M. R., Petr-Gotzens, M. G., & Martín, E. L. 2012, *ApJ*, 754, 30
- Peña Ramírez, K., Zapatero Osorio, M. R., & Béjar, V. J. S. 2015, *A&A*, 574, A118
- Pecaut, M. J. & Mamajek, E. E. 2013, *ApJS*, 208, 9
- Persi, P., Marenzi, A. R., Kaas, A. A., Olofsson, G., Nordh, L., & Roth, M. 1999, *AJ*, 117, 439
- Persi, P., Tapia, M., Gómez, M., Whitney, B. A., Marenzi, A. R., & Roth, M. 2007, *AJ*, 133, 1690
- Petr-Gotzens, M. G., Cuby, J.-G., Smith, M. D., & Sterzik, M. F. 2010, *A&A*, 522, A78
- Rayner, J. T., Cushing, M. C., & Vacca, W. D. 2009, *ApJS*, 185, 289
- Reipurth, B., Mikkola, S., Connelley, M., & Valtonen, M. 2010, *ApJ*, 725, L56
- Robin, A. C., Reylé, C., Derrière, S., & Picaud, S. 2003, *A&A*, 409, 523
- Schmidt, S. J., West, A. A., Bochanski, J. J., Hawley, S. L., & Kietly, C. 2014, *PASP*, 126, 642
- Scholz, A., Geers, V., Clark, P., Jayawardhana, R., & Muzic, K. 2013, *ApJ*, 775, 138
- Scholz, A., Geers, V., Jayawardhana, R., Fissel, L., Lee, E., Lafreniere, D., & Tamura, M. 2009, *ApJ*, 702, 805
- Scholz, A., Jayawardhana, R., Muzic, K., Geers, V., Tamura, M., & Tanaka, I. 2012a, *ApJ*, 756, 24
- Scholz, A., Muzic, K., Geers, V., Bonavita, M., Jayawardhana, R., & Tamura, M. 2012b, *ApJ*, 744, 6
- Scholz, A., Wood, K., Wilner, D., Jayawardhana, R., Delorme, P., Caratti o Garatti, A., Ivanov, V. D., Saviane, I., & Whitney, B. 2010, *MNRAS*, 409, 1557
- Sumi, T., Kamiya, K., Bennett, D. P., Bond, I. A., Abe, F., Botzler, C. S., Fukui, A., Furusawa, K., Hearnshaw, J. B., Itow, Y., Kilmartin, P. M., Korpela, A., Lin, W., Ling, C. H., Masuda, K., Matsubara, Y., Miyake, N., Motomura, M., Muraki, Y., Nagaya, M., Nakamura, S., Ohnishi, K., Okumura, T., Perrott, Y. C., Rattenbury, N., Saito, T., Sako, T., Sullivan, D. J., Sweatman, W. L., Tristram, P. J., Udalski, A., Szymański, M. K., Kubiak, M., Pietrzyński, G., Poleski, R., Soszyński, I., Wyrzykowski, L., Ulaczyk, K., & Microlensing Observations in Astrophysics (MOA) Collaboration. 2011, *Nature*, 473, 349
- Whitworth, A. P. & Zinnecker, H. 2004, *A&A*, 427, 299
- Wilking, B. A., Greene, T. P., & Meyer, M. R. 1999, *AJ*, 117, 469
- Zapatero Osorio, M. R., Béjar, V. J. S., Martín, E. L., Rebolo, R., Barrado y Navascués, D., Bailer-Jones, C. A. L., & Mundt, R. 2000, *Science*, 290, 103
- Zapatero Osorio, M. R., Béjar, V. J. S., & Peña Ramírez, K. 2013, *Mem. Soc. Astron. Italiana*, 84, 926
- Zapatero Osorio, M. R., Gálvez Ortiz, M. C., Bihain, G., Bailer-Jones, C. A. L., Rebolo, R., Henning, T., Boudreault, S., Béjar, V. J. S., Goldman, B., Mundt, R., & Caballero, J. A. 2014, *A&A*, 568, A77
- Zapatero Osorio, M. R., Rebolo, R., Bihain, G., Béjar, V. J. S., Caballero, J. A., & Álvarez, C. 2010, *ApJ*, 715, 1408